ERS-1 and Multifrequency Polarimetric SAR Calibration-Validation Results

Yves-Louis Desnos, Marc Loiselet

European Space Agency, ESTEC
P.O. box 299 - 2200 AG Noordwijk - The Netherlands
Tel: (31) 1719 84927 - Fax (31)1719 84596

ABSTRACT

This paper summarizes some of the activities performed in the European Space and Technological Center of the European Space Agency in the field of SAR data calibration-validation as a support of the development of actual and future spaceborne SAR instruments.
Calibration-validation is a necessary step towards the scientific use of remote sensing data and with the successful launch and operation of ERS-1 satellite, ESA has introduced new calibration standards for SAR thanks to the development and operation of high precision Active Radar Calibrators (transponders).
As a preparation of future spaceborne instruments we have been working on airborne multifrequency polarimetric SAR data. Methodology for calibration and differences compared to classical SAR will be explained. Results from calibration and quality analysis are discussed. ERS-1 data calibration results using transponders are presented and compared with those obtained using corner reflectors. SAR data quality analysis results using point targets are discussed.

Keywords: SAR, calibration, validation, polarimetry, ERS-1

INTRODUCTION

We are now entering a new era where a lot of SAR remote sensing data will be available and calibration-val\-idation is a necessary step for scientific use of the data.
Considering commonalities in tools for calibration and validation of different SAR data and the expertise we have built up in ESTEC, we have developed a workstation dedicated to SAR calibration-validation.

As testbed for our workstation we have chosen the Flev\-oland site located in the Netherlands because ERS-1 trans\-ponders (active radar calibrators) and corner reflectors from JPL and FEL-TNO with their deployment parameters were available (BARNES, 1986). Over this test site we have analysed ERS-1 data coming from different ground processors and NASA DC8 airborne SAR data generated during the European campaigns of 1989.

This paper is splitted into two parts corresponding to the main kinds of products studied. Section I is about the multifrequency polarimetric SAR data (MAESTRO-1 Campaigns), while section II is dedicated to ERS-1 data. In both parts methodologies used for calibration are outlined, quality analysis and calibration results are discussed.

1. MULTIFREQUENCY POLARIMETRIC SAR DATA

Polarimetric SAR for remote sensing applications has been a field of strong activity specially with the European deployment of the NASA/JPL C-, L- and P-band airborne polarimetric SAR in August 1989. This deployment supported and financed by ESA and JRC represented a good opportunity to test and evaluate the capability of multi-frequency polarimetric imaging in the fields of agricultural and forestry applications where an extensive ground data collection has been performed by scientists (BORGEAUD, 1986) (DESNOS, 1991). This deployment represented also an unique opportunity to assess the effect of different levels of calibration on the information extraction from the data.

The data was selected in uncalibrated four looks compressed format (DUBOIS, 1987) and the calibration process divided in different steps: relative phase calibration using the Zebker et al. algorithm (FREEMAN, 1991), cross-talk removal and relative amplitude calibration using the Van Zyl algorithm (GRAY, 1990), absolute calibration and corner reflector analysis using the integral method described by Gray et al. (GROOT, 1990).

Background and hypotheses used in the calibration process are summarized in the following chapter.

1.1 Background and Hypotheses

For both classical and polarimetric SAR systems, absolute calibration permits to determine accurately the back\-scattering coefficient of the target. For polarimetric SAR calibration, it is also necessary to measure amplitude and phase between the four coherent data channels (hh, hv, vh, vv) to perform coherent processing such as polarimetric synthesis. A good design of the instrument may permit to have a good balance between amplitude in the h and v channels and to correct for path differences, but in practice a dedicated calibration is needed to remove remaining relative phase unbalance between the channels and cross-talk between the horizontal and vertical antenna patterns. Furthermore these techniques may permit to relax requirements on critical technological parts of the instrument such as the cross-talk in a patch array antenna (GROOT, 1991).

The quad polarization measurement made by a polarimetric SAR can be written as

$$[E] = Ae^{i\phi}\,[R]\,[S]\,[T] \tag{1}$$

where the elements E_{ij} of the matrix $[E]$ are the complex voltages measured by the radar and $[S]$ is the polarisation scattering matrix of the target. The factor A represents the overall absolute amplitude factor and ϕ the overall absolute phase factor due to the round trip propagation. The matrices $[R]$ and $[T]$ represent the polarisation distortion of the receive and transmit channels of the radar respectively. This distortion of the measured scattering matrix can be characterised by the amplitude and phase mismatch errors and cross-talk coupling in the transmit and receive channels of the radar (HOEKMAN, 1990). The first hypothesis to consider comes from the data themselves. The system is modelled as reciprocal because in the compression process the measured scattering matrix is symmetrized , therefore:

$$[E] = [E]^T \tag{2}$$

We note that the absolute phase factor is "lost" in the synthesis process and that reciprocity in the backscattering mechanism $[S] = [S]^T$ implies that $[R] = [T]^T$ as follows from (1) and (2).

2. RELATIVE PHASE CALIBRATION

To illustrate the methodology used, let us consider the measured scattering matrix $[S]$ for one resolution cell only. Due to the different propagation paths in the radar, the quad polarization measurement takes the following form (FREEMAN, 1985):

$$[E] = \begin{pmatrix} S_{hh}\exp\,[i(\phi_{t,h}+\phi_{r,h})] & S_{hv}\exp\,[i(\phi_{t,v}+\phi_{r,h})] \\ S_{vh}\exp\,[i(\phi_{t,h}+\phi_{r,v})] & S_{vv}\exp\,[i(\phi_{t,v}+\phi_{r,v})] \end{pmatrix} \tag{3}$$

Assuming $\phi_t = \phi_{t,h} - \phi_{t,v}$ and $\phi_r = \phi_{r,h} - \phi_{r,v}$ (3) becomes

$$[E] = \exp\,[i(\phi_{t,v}+\phi_{r,v})] \begin{pmatrix} S_{hh}\exp\,[i(\phi_t+\phi_r]\; S_{hv}\exp\,[i\phi_\rho\,] \\ S_{vh}\exp\,[i\phi_t] \qquad S_{vv} \end{pmatrix} \tag{4}$$

Introducing backscatter reciprocity ($S_{hv} = S_{vh}$), we can solve the differences $\phi_t - \phi_r$ from the complex product $E_{hv}\,E^*_{vh} = S_{hv}\,S^*_{vh}\exp\,[\,i\,(\phi_r - \phi_t)\,]$ averaged over the image. Finally knowing the scattering mechanism at one point in the image (e.g. hh/vv phase difference = 0° for a slightly rough surface) is sufficient to determine $\phi_t + \phi_r$. We are now able to determine the individual phases ϕ_t and ϕ_R and to phase calibrate the measurement:

$$[S] = \begin{pmatrix} E_{hh}\exp\,[-\,i(\phi_t+\phi_r] & E_{hv}\exp\,[-\,i\phi_r\,] \\ E_{vh}\exp\,[-\,i\phi_t] & E_{vv} \end{pmatrix} \tag{5}$$

3. CROSS-TALK REMOVAL

The measured scattering matrix may be written as \break (GRAY, 1990):

$$[E] = Ae^{i\phi}\begin{pmatrix} 1 & \delta_2 \\ \delta_1 & f \end{pmatrix}[S]\begin{pmatrix} 1 & \delta_1 \\ \delta_2 & f \end{pmatrix} \tag{6}$$

where δ_1 (complex number) represents the cross-talk when vertically polarised waves are transmitted or received and δ_2 when horizontally polarised waves are transmitted or received. Noting that:

$$\begin{pmatrix} 1 & \delta_1 \\ \delta_2 & f \end{pmatrix} = \begin{pmatrix} 1 & 0 \\ 0 & f \end{pmatrix}\begin{pmatrix} 1 & \delta_1 \\ \delta_2/f & 1 \end{pmatrix} or\ [T] = [T_c]\,[T_x] \tag{7}$$

In the same manner we can write $[R] = [R_x]\,[R_c]$ with $[R_c] = [T_c]$ (matrix independent of system cross-talk) and $[R_x] = [T_x]^T$. Therefore

$$[E] = [R_x]\,[W]\,[T_x] \tag{8}$$

with

$$[W] = Ae^{i\phi}\,[R_c]\,[S]\,[T_c] \tag{8bis}$$

where $[W]$ contains the only last two steps of calibration, amplitude imbalance and absolute calibration. The matrices $[R_x]$ and $[T_x]$ contain the parameters δ_1 and δ_2/f to

be estimated without relying on external devices. This is done with the following assumptions: δ_1 and δ_2 are small compared to 1 implying the system is well isolated and the co- and cross-components of $[S]$ are uncorrelated as predicted in (LAUR, 1990) which means $<S^*_{hh} S_{hv}> = 0$ and $<S^*_{vv} S_{hv}> = 0$ (which is also true for the elements of $[W]$). To find an estimate of δ_1 and δ_2/f from (8) and under the stated assumptions it is necessary to know $<W_{hv} W^*_{hv}>$ and the measured elements of $[E]$.

An initial value of $\delta_1 = \delta_2/f = 0$ is used to evaluate a first estimate $<W_{hv} W^*_{hv}>$ from (9) and then an initial guess of cross-talk parameters is calculated from (8) and so on until a stable estimate is reached. Hence the cross-talk calibration is obtained by computing the following equation:

$$[W] = [R_x^{-1}]\,[E][T_x^{-1}] \tag{9}$$

4. RELATIVE AMPLITUDE CALIBRATION

Having achieved the levels of calibration that may be performed using the data themselves, the residual amplitude offsets between the channel still remain. These are represented by $|f|$ in (8bis):

$$[W] = Ae^{i\phi}\begin{pmatrix} S_{hh} & f \cdot S_{hv} \\ f \cdot S_{hv} & f^2 \cdot S_{vv} \end{pmatrix} \tag{10}$$

The amplitude of f is measured with (10) using a calibrator with known relation between hh and vv (e.g. trihedral).

5. ABSOLUTE AMPLITUDE CALIBRATION

By comparing the estimated theoretical value of calibrators with the actual values measured in the image using the integral method (GROOT, 1990), we correct for an estimated gain offset to absolutely calibrate the data.

5.1 Calibration Methodology and Results

We have chosen from the Maestro-1 data set the Flevoland 116 track available in C- and L-band where four square based trihedral corner reflectors were deployed. The deployment parameters of the trihedrals are from reference (BORGEAUD,1986).

- 1) The first step of the calibration process we perform is the corner reflector analysis. The pixel positions of the corner reflectors are manually located (either in the hh or vv image). For each corner reflector we determine the parameter f (phase and amplitude), the integrated signal to background ratio S/C and the absolute calibration factor. This analysis provides us ideally with information on the relative phase error $arg(f)$ to be removed, the relative amplitude offset $|f|$, and to a certain extent on the calibrability of the data, i.e. is the *signal/background* high enough.

Table 1 gives the results of corner reflector analysis for the C- and L-band image that we will compare to worst case theoretical errors ε derived from SNR (11)(12)(13) (when calibrators orientation, manufacturing and other aircraft induced errors are not considered).

$$\varepsilon\,[\,|f|\,] = [1 + - 4/(SNR)^{1/2}\,]^{1/4} \tag{11}$$

$$\varepsilon\,[arg\,(f)\,] = \pm \tan^{-1}\,(2/(SNR)^{1/2} \tag{12}$$

$$\varepsilon\,[\,absolute\ gain\,] = [1 \pm 2/(SNR)^{1/2}\,]^{1/2} \tag{13}$$

- 2) Now let us proceed with the calibrattion as if no calibrators wer deployed on the site. In view of phase calibrating the data we can determine the histogram of the hh and vv phase difference. By representing in grey levels or colour the phase difference at each pixel we can select an area with uniform phase properties. The actual amplitude image helps us to identify an area

Table 1: Corner reflector analysis and worst case theoretical error ε.

incidence angle [degree]	$\|f\|$		arg(f) [degree]		absolute gain [dB]		S/C [dB]	
	L-Band	C-Band	L-Band	C-Band	L-Band	C-Band	L-Band	C-Band
40.19	1.0543	1.0041	−17.25	−52.02	9.58	9.99	20.95	28.35
49.87	0.9418	1.0729	−18.25	−50.86	7.21	8.02	16.68	27.57
50.54	0.9551	1.1037	−17.86	−56.10	7.92	4.90	24.04	28.70
51.38	0.9372	1.0674	−19.77	−56.22	9.15	10.34	21.10	30.53
error ε								
min	0.91	0.96	− 5.7	− 2.0	− 1.0	− 0.16	SNR =	SNR =
max	1.12	1.03	+ 5.7	+ 2.0	+ 0.8	+ 0.15	20 dB	29 dB

where the scattering mechanism is known (e.g. water, slightly rough surface). When these two conditions are met we can perform relative calibration.

We have actually performed phase calibration using the water area image at the top right corner of the image. The *hh/vv* difference phase histogram shows a strong correlation and is therefore ideal for phase calibrating the data.

Figure 1a shows an uncalibrated co-pol signature of a corner reflector in L- and C-band. Figure 1b presents the results after phase calibrating the data using clutter statistics. These results are confirmed by the results shown in figure 1 c using corner reflectors to phase calibrate the data. We obtained similar results in L-Band while using selected fields to phase calibrate the data using clutter statistics. In C-band phase calibration is performing less well due to along track HH/VV phase variation observed on the data set.

- 3) Next step is the cross-talk removal. As cross-talk is only a function of range, an average value of cross-talk parameters is estimated by iteration as described range line per range line: 128 estimates of 8 adjacent pixels are used to estimate the cross-talk of the line.

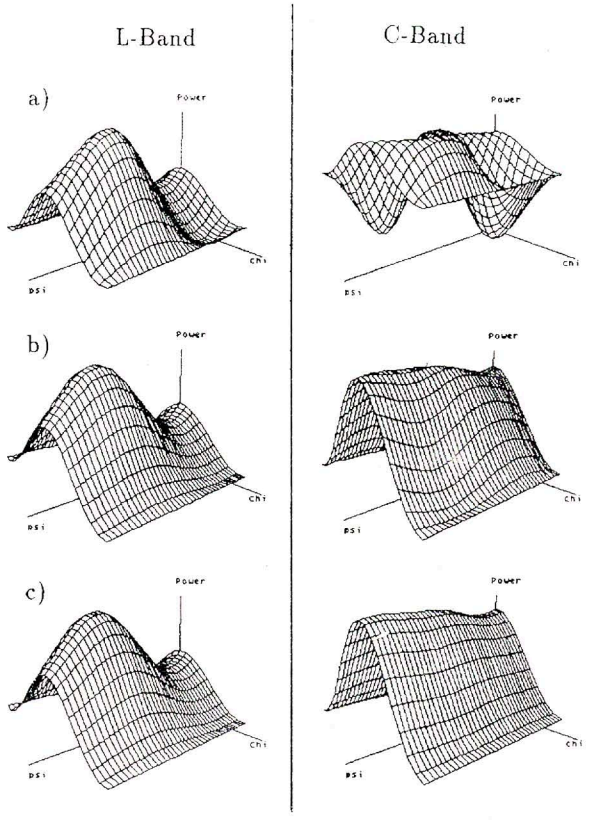

Fig. 1 - Co-polarized signature of the same triedral a) uncalibrated; b) calibrated using phase statistic; c) Calibrated using corner reflector average difference.

The results in L-Band of cross-talk amplitude are plotted in figure 2 and show a very good agreement with the measurements on the real antenna in figure 3. By analysis of signatures before cross-talk calibration figures 4 a ,\ 4b we clearly see the distortion effect of a higher cross-talk for low incidence angle. In figure 4 a, 4b we notice an improvement of the L-band corner reflector signature after calibration.

In C-band, cross-talk calibration shows very little improvement in the signature ure 4 c as expected considering the level of cross-talk extracted from the data ranging from -20 *dB* to -30 *dB* in figure 2.

- 4) Relative amplitude calibration is performedby measuring |f| using corner reflectors. This measurement is performed using the power ratio of *hh/vv* integrated over a cross-shaped area centered on the corner reflector. This measured |*f*| is used to correct the remaining channel amplitude imbalance (f^2 between *hh/vv* and *f* between *hh/hv*).

The reason that this calibration method is only partially successfull is due to the sensitivity of SNR (11). In L-band the SNR is ~ 20 *dB* while at C-band, the SNR is ~ 29 *dB* (see Table 1).

- 5) For absolute calibration, an average absolute calibration factor is calculated from the different calibrators using the integral method which relates "point to distributed targets power":

$$\sigma_0 = \frac{\sigma \sin \theta}{\delta_r \, \delta_a \, C_i} \tag{14}$$

By correcting the backscatter (power) of each pixel by this factor we absolutely calibrate the data.
Absolute calibration factors are given in Table 2. The results show to be in good agreement with those published in (VAN ZYL, 1990).

Table 2: Radiometric bias factors comparison.

BAND	L-banb (dB)	C-band (dB)
ESA Flevoland (HH-track 116)	-22.4	-24
JPL Flevoland (HH-track 056)	-21.7	-23.4
JPL Bias estimate (HH)	-22.9 (+/- 1.2)	-24 (+/- 0.7)

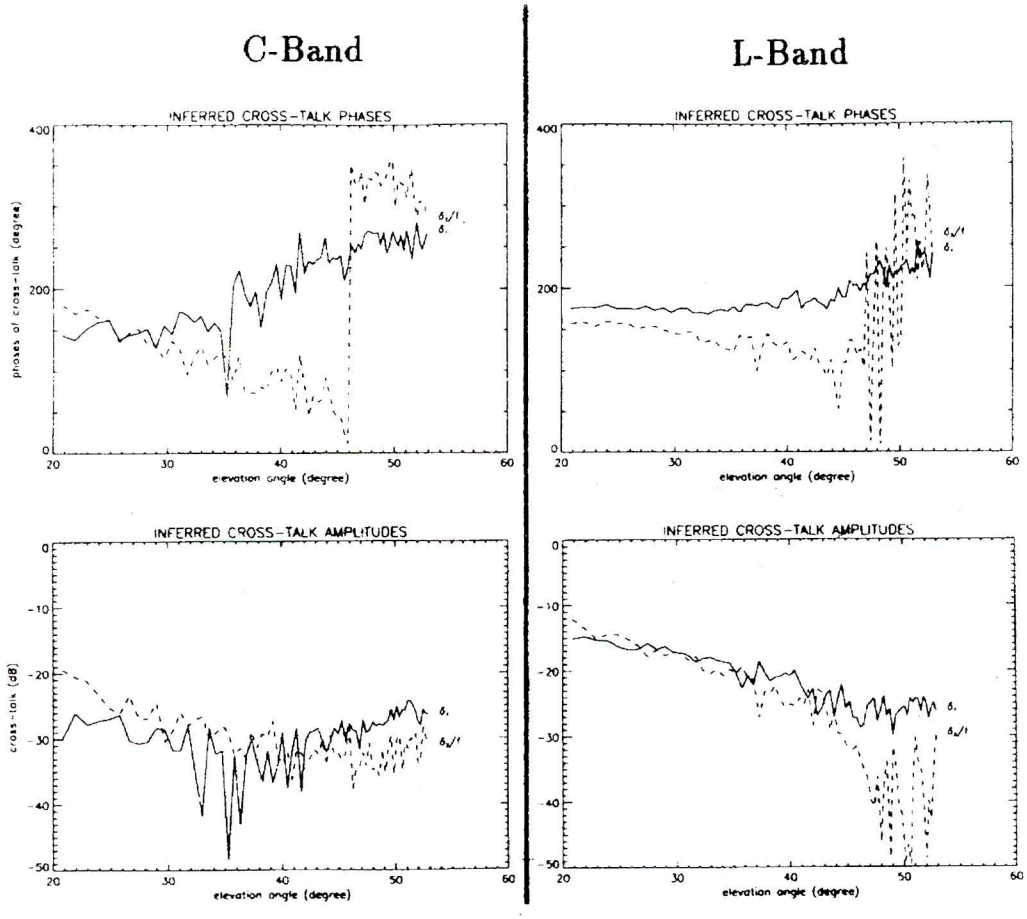

Fig. 2 - Amplitude and phase of cross-talk parameters δ_1 δ_2/f inferred from the data as a function of elevation angle.

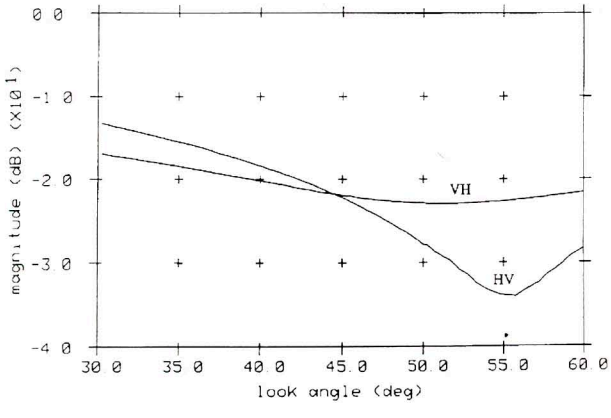

Fig. 3 - Measured L-Band SAR Antenna cross-talk.

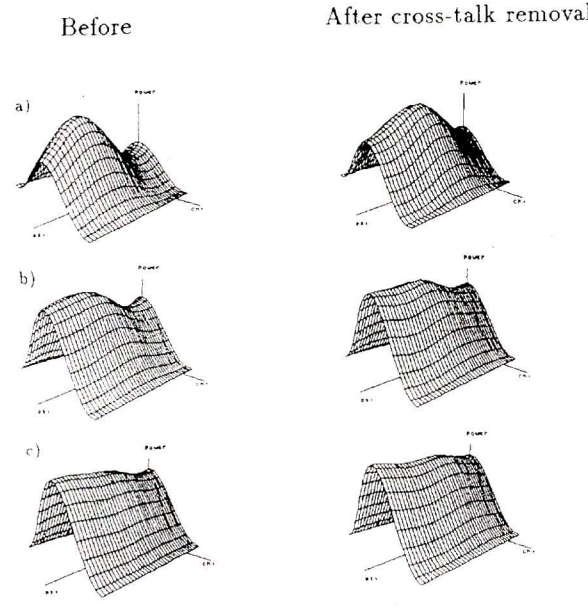

Fig. 4 - Effect of cross-talk removal illustrated by copolarized signature of phase calibrated corner reflector a) L-Band 50 degrees incidence; c) C-Band 40 degrees incidence.

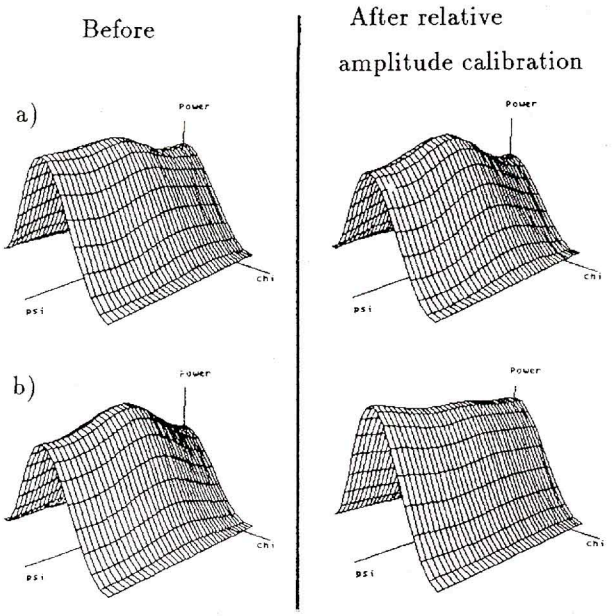

Fig. 5 - Effect of relative amplitude calibration illustrated by signature of phase / cross-talk calibrated triedral: a) L-band; b) C-Band.

6. QUALITY ANALYSIS

6.1 Definition of the parameters

Quality analysis has been done using the four trihedral corner reflectors from the Flevoland 116 track. The impulse reponse function (IRF) is obtained by selecting an area of 32x32 pixels around the main peak; then this area is interpolated with a factor equals to 8 in both directions. The interpolation is done in two dimensions by a Hanning multiplication, FFT, zero-fill, IFFT and Hanning division. The following parameters are computed:

Resolution: azimuth (range) resolution is classically defined as the 3dB-width of the IRF along the azimuth (range) axis. Those two numbers define the resolution cell as a rectangle which sides are equal to the azimuth and range resolutions. The resolution cell is used to calculate the integrated side lobe ratio (ISLR and NISLR).

Peak side lobe ratio (PSLR): azimuth (range) PSLR is defined as the ratio of the intensity of the main peak to the highest first peak, following the azimuth (range) axis. The value is given in dB.

Normalised Integrated side lobe ratio (NISLR): 2D NISLR is defined as the ratio of the energy per resolution cell within a rectangle centred on the point target and of dimensions 10x10 resolution cells, but excluding the main lobe area of dimensions 2x2 resolution cells, to the energy per resolution cell in the main lobe area. Azimuth (range) NISLR is defined as the ratio of the energy per resolution cell in the main lobe of 2x2 resolution cells, to the energy per resolution cell in a rectangle of 2x10 resolution cells following the azimuth (range) axis but excluding the main lobe. ERS-1 ISLR definition uses the same area but without normalising data by the number of resolution cells.

Signal to clutter: the clutter value in dB is the mean of the amplitude in each corner (8x8 pixels) of the 32x32 pixels vicinity centred on the point target. Then the signal to clutter is defined as the ratio of the amplitude of the maximum interpolated to the clutter.

6.2 Application and results on MAESTRO-1 DATA

The results for three corner reflectors from a VV polarised image acquired over Flevoland in August 1989 are displayed in Table 3. In L-band the average azimuth (range) resolution is 15.2 metres (9.5 metres). For C-band, we get respectively 12.3 and 8.7 metres. The NISLR are roughly -9 dB in L-band and -18 dB in C-band.

7. ERS-1 DATA

With the successful launch and in orbit operation of the first European Remote Sensing Satellite ERS-1, ESA is able to provide scientists of the world, thanks to the Synthetic Aperture Radar instrument, unique data sets for sea ice, coastal area and land ressources management. ERS-1 is a forunner of a new generation of space missions in the 1990's and will be followed by other European Earth Observation Satellite (ERS-2, Polar Platform) and some non European projects RADARSAT, SIR-C etc.

7.1 Quality Analysis

Using definitions and methods presented before we show in Table 4 the results from a data set acquired on 18th and 27th November over Flevoland and processed in fast delivery format respectively in the Kiruna (SWEDEN) and Tromso (NORWAY) satellite station. Values presented here are averaged over 5 different JPL corner reflectors. These results first highlight the stability of the instrument which can be seen on the integrated peak energy. One notices differences on ground range resolution and range PSLR which illustrate two possible trade-off in term of spatial resolution versus Peak Side Lobe Ratio and differences in ground range resampling algorithm.

Table 3: Quality analysis results on Flevoland data in VV polarisation; ISLR are normalised.

Frequency	L-band		C-band	
FEL-TNO	CR1	CR2	CR2	CR3
az. resolution	15.77 m	14.68 m	12.27 m	12.39 m
ra. resolution	10.08 m	8.88 m	8.58 m	8.75 m
azimuth PSLR	- 11.9 dB	- 11.1 dB	- 15.3 dB	- 14.0 dB
range PSLR	- 12.5 dB	- 9.9 dB	- 17.6 dB	- 16.8 dB
2D NISLR	- 9.3 dB	- 9.3 dB	- 18.2 dB	-18.9 dB
azimuth NISLR	- 9.5 dB	- 9.5 dB	-15.1 dB	- 14.5 dB
range NISLR	- 9.8 dB	- 8.5 dB	-17.4 dB	- 17.7 dB

Table 4: Quality analysis on corner reflectors in ERS-1 FDP images.

JPL ΔRC	ground station	3 dB width [m]		int. peak energy [dB]	PSLR [dB]		ISLR [dB]	S/C [dB]
		gr. range	azimuth		range	azimuth		
18 Nov	Tromso	26.03	21.75	89.04	- 15.59	- 16.54	- 0.37	19.96
27 Nov	Tromso	26.89	22.89	89.52	- 15.18	- 17.04	- 1.63	20.99
18 Nov	Kiruna	29.16	21.25	107.66	- 17.58	- 16.97	- 0.76	20.41
27 Nov	Kiruna	29.49	20.91	107.32	- 18.43	- 17.85	- 1.86	21.47

8. CALIBRATION METHODOLOGY AND RESULTS

8.1 Calibration methodology

When compared to Polarimetric SAR, in the ERS-1 case only the last step of calibration is necessary: absolute calibration. Three different methods for estimating the absolute radiometric bias factor have been developed: the peak method, the integration method on pixel values, the integration method on interpolated values.

a) Peak Method

This method uses estimates of the peak pixel value of the impulse response of a known radar reflector to derive the backscatter coefficient of adjacent clutter areas. This leads to the calculation of

$$\sigma^0 = \frac{\sigma}{P_p \cdot \rho_r \cdot \rho_a} \cdot \sin\theta_u \cdot P_u \tag{15}$$

where σ is the RCS of the known point target, P_p is the peak reflector estimate, ρ_a and ρ_r are the azimuth and slant range resolutions respectively, and θ_u is the local incidence angle of the uniform distributed target with the average pixel value P_u (background contribution is assumed negligible). In this equation the factor

$$C_p = \frac{P_p \cdot \rho_r \cdot \rho_a}{\sigma} \tag{16}$$

is only depending on the calibration device and not on the distributed target. Hence, it can be regarded as the general calibration factor for the peak method. The shape and peak value of the impulse response function of a point target such as a reflector depends on how well the linear FM rates are matched and on the form of the reference function weighting used to reduce the sidelobes Table 4. The aver-

age pixel value P_u for a uniform clutter area is independent of focus, but the peak impulse value P_p is not.

b) Integration Method on Pixel Values

This method integrates the power of the calibration device (i.e. corner reflector or transponder) in an area around it. This calculation includes the sum of the point target power as well as the power received from the background of the area. Therefore the background contribution has to be subtracted. This can be done by averaging the background power over an area without dominant point targets to estimate the background in the integration area. The calculation of the integrated reflector energy P_{i+} is done on the crossshaped integration area (N = 189 pixels) around the point target. The background contribution is estimated by the 4 square areas $M = 5 \times 5$) in the corners of the cross. Thus, the background corrected integrated power can be calculated as

$$P_{i+} P_{+} - \frac{N}{4 \cdot M} \cdot P_{clutter} \tag{17}$$

This leads to the calculation of

$$\sigma^0 = \frac{\sigma}{P_{i+} \cdot \delta_r \cdot \delta_a} \cdot \sin \theta_u \cdot P_u \tag{18}$$

where σ is the RCS of the known point target, P_{i+} is the integrated reflector energy, δ_a and δ_r are the image azimuth and slant range pixel spacings respectively, and θ_u is the local incidence angle of the uniform distributed target with the average pixel value P_u. In this equation the factor

$$C_{i+} = \frac{P_{i+} \cdot \delta_r \cdot \delta_a}{\sigma} \tag{19}$$

is only depending on the calibration device and not on the distributed target. Hence, it can be regarded as the general calibration factor for the integrated method on pixel values. This integration method has major advantage to be independent of processor focus or actual resolution.

c) Integration Method on Interpolated Values

This method, proposed in (WOODE, 1992), is very simular to the previous one with the exception of the calculation of the integrated energy. Here the integrated energy is computed on interpolated values by summing the pixel intensities over a square region (N interpolated pixels with $N = 31 \times 31$) surrounding the peak location. Of course this value has to be corrected by an estimation of the clutter which is calculated in a border (larger square region of M interpolated pixels with $M = 51 \times 51$) surrounding the peak location. Hence, the background corrected integrated energy is

$$P_{ii} = \sum^{N} |A|^2 - \frac{N}{M-N} \cdot \left(\sum^{M} |A|^2 - \sum^{N} |A|^2 \right) \tag{20}$$

This leads to the general calibration factor of the integration method on interpolated values

$$C_{ii} = \frac{P_{ii} \cdot \delta_r \cdot \delta_a}{\sigma \cdot f_{int}^2} \tag{21}$$

where f_{int} is the interpolation factor. Hence, the formula to calibrate an uniform area is

$$\sigma^0 = \frac{\sigma \cdot f_{int}^2}{P_{ii} \cdot \delta_r \cdot \delta_a} \cdot \sin \theta_u \cdot P_u \tag{22}$$

8.2 Application to ERS-1

As foreword one should notice that slant range images should be used for proper calibration. However the methods described above might be applied to ground range images by substituting in (18) and (22) δ_r by $\delta_{gr} \cdot \sin \theta_c$ where δ_{gr} is the ground range pixel spacing and θ_c the incidence angle of the calibrator. After proper compensation for antenna pattern variation and range spreading loss an absolute calibration factor A might be derived from the general calibration factor for each method.

Table 5 shows some averaged general calibration factors derived using the three methods presented above, respectively from four JPL corner reflectors deployed in a same field in Flevoland on the 18th and 27th November 1991 data sets from Tromso. One can notice good agreement between the two integral methods.

8.3 Transponders versus corner reflectors

On ERS-1 images of the Flevoland corner reflectors and transponders have been deployed at the same time.

a) Cross calibration

In Table 6 cross calibration experiment performed using three transponders (signal to background = 35 dB, calibration accuracy of +/-0.07 dB) versus 5 JPL corner reflectors

Table 5: Average general calibration factor for JPL corner reflectors.

Date	JPL	Calibration factor peak method	Calibration factor integral method	Calibration factor interpol. method
18 Nov	mean	48.30 dB	48.60 dB	48.50 dB
	std_deviation	0.47 dB	0.82 dB	0.62 dB
27 Nov	mean	48.67 dB	49.28 dB	49.39 dB
	std_deviation	0.45 dB	0.45 dB	0.23 dB

Table 6: JPL corner reflectors versus transponders offsets.

JPL versus Transponders OFFSETS	Peak method (dB)	Integral method on pixels (dB)	Integral method on interpol. values (dB)
18 NOV 91	3.1	2.7	2.7
27 NOV 91	1.8	2.3	2.3
AVERAGE	2.45	2.5	2.5
ESTIMATED OFFSET = 2.5 dB -> estimated JPL corner RCS = 44.16 dBm2			

(signal to background = 20 dB, not calibrated) indicates, whatever the calibration method used, an offset of 2.5 dB on the absolute calibration factor. This shows (neglecting other error sources) that corner reflectors actual radar cross section is 2.5 dB lower than theoretical value given by the length of the reflector. This might be explained by edge effect and flatness problems.

b) Overall stability measurement

The data set used cover a period of 60 days, starting on October 10th 1991. Figure 6 illustrates relative variation measurements of the calibrators RCS versus time. On one hand the transponders (indicated as TP on figure 6) show a very little variation versus time which illustrates the high stability of ERS-1 instrument. On the other hand corner reflectors even surveyed at regular intervals indicates in comparison strong variations due mainly to pointing errors (wind effect), background contribution, ...

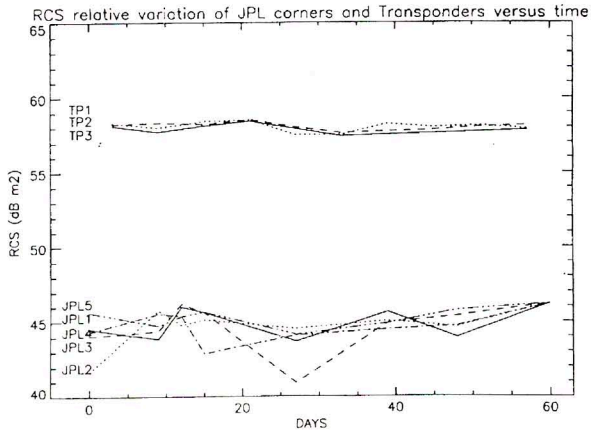

Fig. 6 - RCS relative variation of corners and Transponders versus time.

CONCLUSIONS

We have assessed on an arbitrary site the efficiency of polarimetric calibration procedures in L- and C-band and discussed the weak points. Futhermore, we have performed quality analysis on corner reflectors deployed in Flevoland fields. The results point out a good agreement between the calibrators responses.

Using ERS-1 active radar calibrators (transponders) we are able to calibrate SAR images with very high accuracy for a very long period of time independantly of any survey or meteorological conditions. Using corner reflectors data quality analysis and calibration might be performed provided their alignement towards the radar has been checked, their radar cross section is accurately known and their signal to background is high enough.

This work is part of an overall calibration/data exploitation activity in view of supporting the technical definition and development of future SAR instruments within ESA.

ACKNOWLEDGMENTS

We would like to thank E. Attema, J.-P. Guignard and D. Maccoll (ESA) for their support and comments doing this work. We specially thank A. Freeman and L. Harrison from JPL for providing us with the Polcal software and many data sets from the JPL airborne SAR. The help of J. Groot (FEL-TNO Holland) in providing calibrators deployment parameters has been highly appreciated. Polarimetric synthesis of the data has been done using Poltool software developed by JRC. We want also to thank J. Lichtenegger from ESA/ESRIN for his work distributing Maestro-1 data and D. Hoekman for fruitful discussion on MAESTRO-1 calibration results, S. Minde, E. Elligsen from Tromso Satellite Station and I. Petiteville, C. Caspar, H. Laur(ESA) for ERS-1 data distribution.

REFERENCES

Barnes , R.,1986, Polarimetric radar calibration using in sce\-ne reflectors. report TT-65, Lincoln Laboratory, Lexington(MA).

Borgeaud , M., et al., 1987, Theoretical models for polarimetric radar clutter. J. Electromagn. Waves Appl., vol 1, 67-86.

Desnos, Y.-L., Borgeaud, M., and, Seifert, F. -M.,1991, Effect of calibration on the extraction of information from Polarimetric Maestro-1 SAR data. \break IGARSS'91.

Dubois, P., and Norikane, L., 1987, Data volume reduction for imaging radar polarimetry. in Proc. IGARSS'87, 691, 696.

Freeman, A, Shen, Y., Van Zyl, J., and Klein, J. D., 1991, Calibration of NASA/JPL DC-8 SAR data. IGARSS'91, vol 3, pp. 1377-1379.

Gray, L, et al.,1990, Synthetic Aperture Radar calibration using reference reflectors. IEEE GRS, GE-28, 374-383.

Groot, J., and Freeman, A.,1990, Maestro-1, Data Workshop \ Proceedings. ESA-JRC IRSA/MWT/4.90.

Groot, J., and Van Den Broek B., 1991, Trihedral deployment in the Flevopolder for ERS-1 SAR calibration. Fax to ESA/ESTEC.

Hoekman, D., 1990, Maestro-1, Data Report. ESA-JRC Report number IRSA\-/MWT\/1.90.

Laur, H. et al, 1990.Technical note ECISAR Test Image - Quality Analysis and Calibration results. Document number ER-TN-EPO-GP-1901,ESA Publication Division.

Van Zyl , J.-J., 1990, Calibration of polarimetric \break radar images using only image parameters and trihedral corner reflector responses. IEEE GRS, GE-28, pp. 337-348.

Woode, A., Desnos, Y.-L., and H. Jackson, H., 1992, The development and provisional results from the ESTEC ERS-1 Active Radar Calibration Unit. IEEE Geoscience and Remote Sensing special issue on SAR calibration.

Zebker, H., and Lou, Y.,1990, Phase calibration of imaging radar polarimeter stokes matrix. IEEE GRS, GE-28, 246-252.